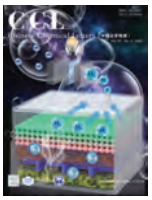
Chinese Chemical Letters 37 (2026) 111351

Contents lists available at ScienceDirect

Chinese Chemical Letters

journal homepage: www.elsevier.com/locate/cclet



Biomimetic NIR-II fluorescent probe from covalent encapsulation enables high-performance NIR-II bioimaging

Zijian Jiang[a,b,c,1], Yijing Du[b,c,1], Zetao Dang[b,c,1], Tongze Liu[a], Mengyuan Liu[b,c], Bin Sun[b,c], Feiran Zhang[b,c,*], Jiajun Xu[a,b,c,*], Shoujun Zhu[b,c,*]

[a] *Key Laboratory of Medicinal Chemistry and Molecular Diagnosis of the Ministry of Education, Key Laboratory of Chemical Biology of Hebei Province, College of Chemistry and Materials Science, Hebei University, Baoding 071002, China*
[b] *State Key Laboratory of Supramolecular Structure and Materials, Center for Supramolecular Chemical Biology, College of Chemistry, Jilin University, Changchun 130012, China*
[c] *Joint Laboratory of Opto-Functional Theranostics in Medicine and Chemistry, The First Hospital of Jilin University, Changchun 130021, China*

ARTICLE INFO

Article history:
Received 8 January 2025
Revised 9 May 2025
Accepted 19 May 2025
Available online 20 May 2025

Keywords:
NIR-II fluorescence imaging
NIR-II cyanine dye
Albumin
Covalent encapsulation strategy
In-vivo imaging

ABSTRACT

To promote the advantages of near-infrared-II (NIR-II) imaging, researchers have developed various types of NIR-II imaging contrast agents, with conjugated dyes being one of the most important categories. However, hydrophobic dyes often rely on encapsulation with amphiphilic polymers for biological applications, which lead to brightness quenching and instability *in vivo*. To address this, we proposed a covalent encapsulation strategy to transform the hydrophobic dye from organic solvent to aqueous solution. To achieve this, we designed a chlorine-containing NIR-II cyanine dye (C7–1080), which covalently binds to human serum albumin (HSA), forming a stable NIR-II fluorescent probe, HSA@C7–1080. The HSA@C7–1080 has precise molecular weight and spatial structure, making dye monodispersing in the albumin pocket with improved fluorescence and stability. This NIR-II fluorescent probe provides high-resolution NIR-II imaging in various biological systems. Our strategy offers a promising alternative for the clinical translation of hydrophobic NIR-II dyes, improving their biocompatibility and imaging performance in fluorescence-guided surgery.

© 2026 Published by Elsevier B.V. on behalf of Chinese Chemical Society and Institute of Materia Medica, Chinese Academy of Medical Sciences.

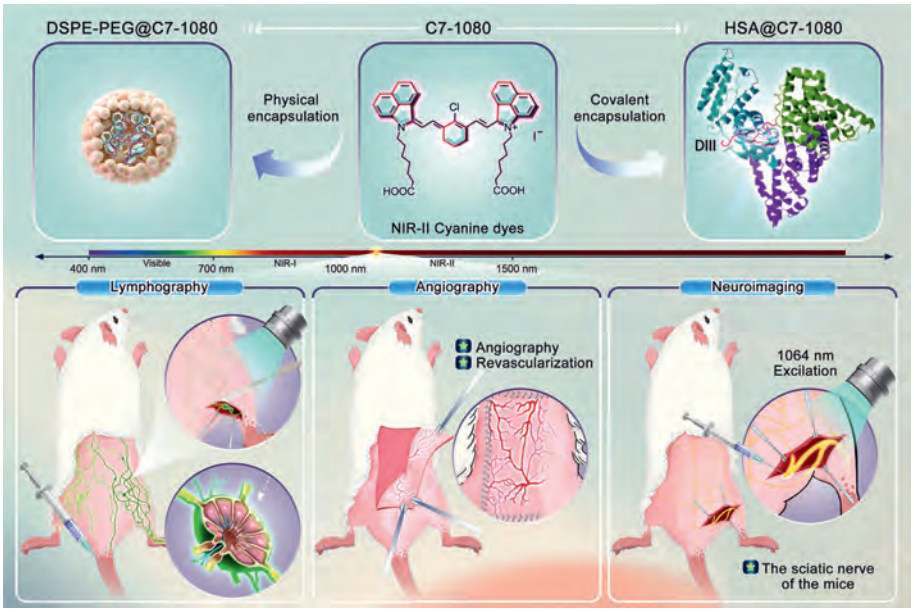
Due to the weak scattering of near-infrared II (NIR-II, >900 nm) fluorescence in various living tissues and the minimal autofluorescence of these tissues [1–5], this region offers deeper imaging depth and higher imaging resolution, making it significant for applications in disease diagnosis and fluorescence-guided surgery [6–9]. Starting with the first-generation NIR-II fluorophore, single-walled carbon nanotubes [10], significant efforts have been made to expand the library of NIR-II fluorophores by incorporating nanomaterials, such as rare earth nanoparticles and quantum dots [11–15]. However, clinically relevant imaging exclusively adopts small molecules. For this reason, organic small molecules, which benefit from good biocompatibility and tunable structures, have increasingly become a research focus in recent years [16–24]. The most successful case in clinical applications to date is indocyanine green (ICG) [6,7].

Although promising in the clinical setting, with several clinical trials underway for other cyanine dyes like IRDye800CW and ZW800–1, a major challenge faced by organic dyes capable of emitting NIR-II fluorescence is their typically large conjugated backbones, which are generally hydrophobic [25–28]. This hydrophobicity complicates their delivery *in vivo*, blood circulation, and accumulation in targeted sites. Classic strategies to address this issue include hydrophilic modifications of the dyes or assembling the dyes with amphiphilic polymers through non-covalent interactions to form nanoparticles for delivery into living organisms [29–35]. Nevertheless, this non-covalent dye encapsulation strategy often lacks control, with structures that are difficult to characterize clearly and relatively poor stability *in vivo*.

Serum proteins serve as carriers for transporting numerous small molecules, such as fatty acids and exogenous drugs [36–39]. The encapsulation of organic small-molecule dyes by albumin regulates their hydrophobicity and enhances their *in vivo* stability and fluorescence intensity, addressing the challenge of *in vivo* delivery. Inspired by this biological phenomenon, a class of chlorine-containing cyanine dyes has been developed that can enter the hydrophobic cavities of various proteins through supramolecular

* Corresponding authors.
E-mail addresses: zhangfr21@mails.jlu.edu.cn (F. Zhang), jjxu_bio@hbu.edu.cn (J. Xu), sjzhu@jlu.edu.cn (S. Zhu).
[1] These authors contributed equally to this work.

https://doi.org/10.1016/j.cclet.2025.111351
1001-8417/© 2026 Published by Elsevier B.V. on behalf of Chinese Chemical Society and Institute of Materia Medica, Chinese Academy of Medical Sciences.



Scheme 1. HSA@C7–1080 NIR-II fluorescent probes constructed using a novel albumin covalent encapsulation strategy for high-precision *in-vivo* visualization of multiple biological events.

interactions [40–42]. Under mild conditions, these dyes can undergo nucleophilic substitution reactions with thiol groups within the proteins, forming covalent bonds and resulting in biomimetic fluorescent probes. This covalent, 1:1 dye-protein encapsulation and delivery strategy offer a more defined structure, better monodispersity, superior fluorescence enhancement, and higher stability *in vivo*. However, this strategy relies on chlorine-containing cyanine dyes that can chemically react with proteins. Currently, widely reported dyes such as IR-780 and IR-808 primarily achieve fluorescence imaging in the NIR-II region through tail emission [43]. Unfortunately, this tail emission results in relatively low quantum yield and poor photostability, significantly limiting the development of this strategy. Although there are many commercially available or reported chlorine-containing cyanine dyes that can extend their fluorescence emission peaks into the NIR-II region, these dyes generally exhibit weak covalent binding capabilities with proteins [17]. Consequently, the fluorescence enhancement effects under covalent encapsulation strategies are not significant.

In this study, we designed and synthesized a chlorine-containing cyanine dye, C7–1080, which has both absorption and emission peaks in the NIR-II region. Compared to existing chlorine-containing cyanine dyes with emission peaks in the NIR-II range, C7–1080 can covalently bind with human serum albumin (HSA), forming a brighter and more stable biomimetic NIR-II fluorescent probe, HSA@C7–1080. Unlike nanoparticles formed through the previously used encapsulation of amphiphilic polymers, this biomimetic NIR-II fluorescent probe can achieve high-resolution NIR-II imaging in various scenarios, including the lymphatic system, vascular system, and nervous system (Scheme 1). Our work provides an alternative strategy for converting hydrophobic NIR-II dyes into hydrophilic ones, thereby enhancing their biocompatibility and holding potential for both fundamental research and clinical applications.

To begin with, we synthesized a chlorine-containing cyanine dye, C7–1080 (Figs. S1-S4 in Supporting information), which has an absorption peak at 1046 nm and an emission peak at 1089 nm in the NIR-II region (Fig. S6b in Supporting information), based on the pioneering work of FD-1080 [17]. The alkyl chain length of C7–1080 was a systematically optimized result for enhanced albumin-binding efficiency and NIR-II brightness (Fig. S5 in Supporting information), building on our previous NIR-II fluorescent probes [44]. This type of chlorine-containing cyanine dye has been widely reported to exhibit good covalent binding capacity with albumin and improved photoluminescence and photostability [40]. For dyes with suitable chemical structure and under normal physiological conditions (37 °C), cyanine dyes can enter the hydrophobic cavities of albumin through supramolecular assembly and undergo nucleophilic substitution reactions with thiol groups to form covalent links, but the required reaction time is relatively long, resulting in low binding efficiency. Therefore, to find a more efficient method for constructing HSA@C7–1080 probes, we screened the reaction conditions and determined that an optimal incubation condition of 60 °C for 2 h provided the best results (Figs. S7-S9 in Supporting information).

Compared to C7–1080, which exists in aggregated form in the aqueous solution (*e.g.*, PBS), the C7–1080 in the HSA@C7–1080 probes "mono-disperses" in the hydrophobic cavities of the albumin in a 1:1 ratio. The chromophore C7–1080 is not only well-dispersed but also exhibits a redshift in both absorption and emission peaks (Figs. S6a and b in Supporting information). In addition, the hydrophobic cavity reduces its interactions with solvent molecules and suppresses the nonradiative transition process (*e.g.*, rotation and vibration), significantly enhancing its fluorescence intensity and photostability (Figs. S6c and d in Supporting information). To demonstrate that C7–1080 is more suitable for constructing biomimetic NIR-II fluorescent probes, we conducted a comparative screening of C7–1080 with three commonly used commercial cyanine-type NIR-II dyes and two previously reported NIR-II dyes known for their ability to bind with albumin (Fig. 1a). Under the same incubation conditions, C7–1080 exhibited the highest fluorescence intensity upon binding with the protein, showing an enhancement of up to 59.28 times compared to the commercial dye IR-1061, and a 2.41-fold increase relative to the widely reported FD-1080 dye (Figs. 1b-d).

To ensure that the HSA@C7–1080 probes can better meet the high-concentration requirements for subsequent *in vivo* imaging, we adopted a low synthesis concentration followed by ultrafiltration concentration. Specifically, we conducted a 1:1 reaction incubation of the dye and albumin at a low concentration of 10 μmol/L to promote sufficient binding between the dye and protein. This

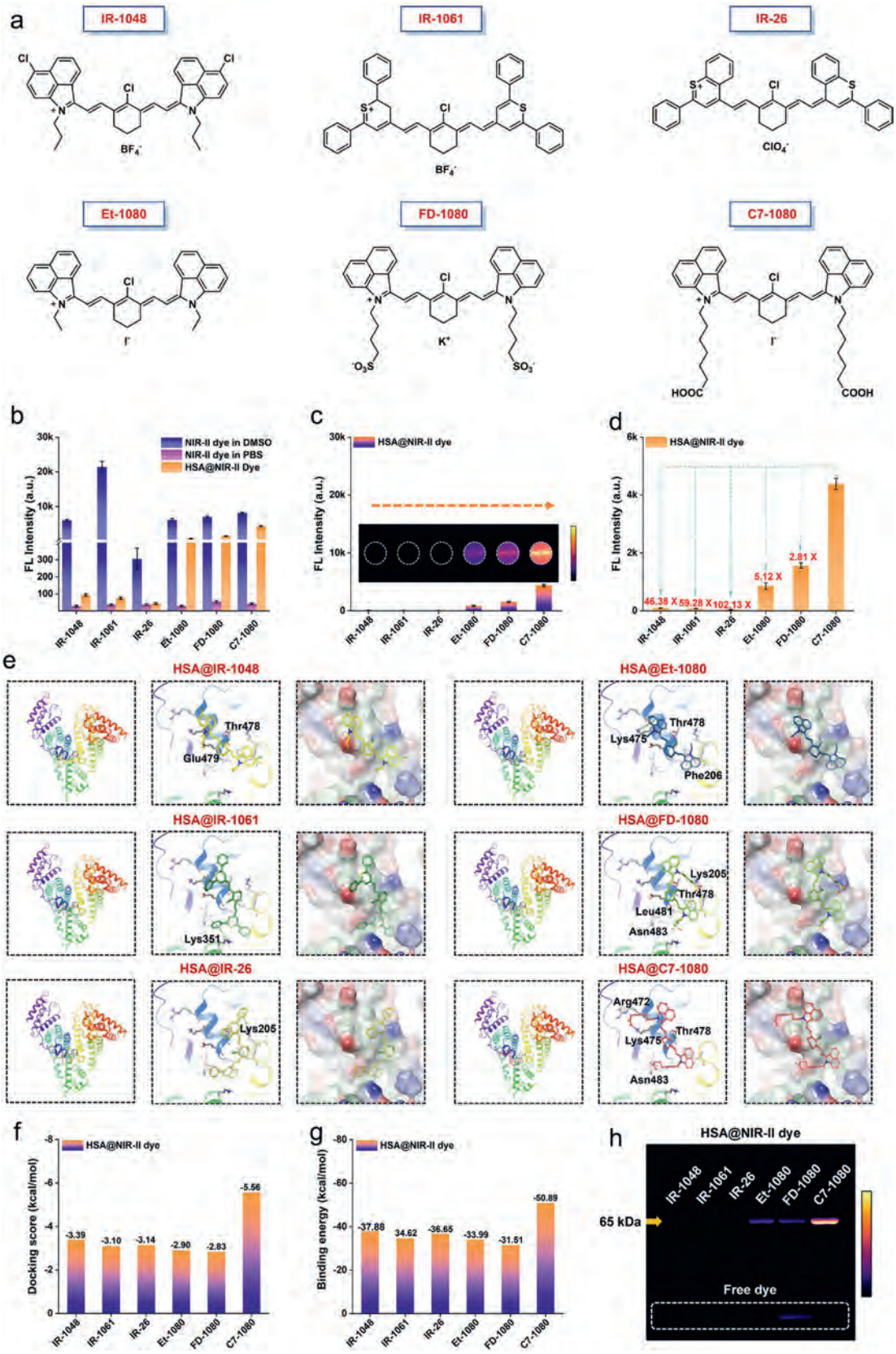


Fig. 1. Binding behavior of various NIR-II dyes with proteins. (a) Chemical structure formulas of the previously reported NIR-II dyes (IR-1048, IR-1061, IR-26, Et-1080, and FD-1080) and the newly designed dye C7–1080. (b) Fluorescence intensity of NIR-II dyes in different solutions, including DMSO, PBS, and HSA solution. (c, d) Fluorescence enhancement effect of different HSA@NIR-II dye complexes. (e) Theoretical simulation of HSA binding to different NIR-II dyes by gliding docking mode. (f, g) Comparison of docking score and binding energy between HSA and different NIR-II dyes. (h) Gel electrophoresis analysis of different HSA@NIR-II dye complexes.

solution was then subjected to ultrafiltration concentration to obtain a higher concentration fluorescent probe solution for *in vivo* injection (Fig. S9g in Supporting information). When the incubation concentration was increased to 20 μmol/L, a noticeable non-linear brightness relative to concentration was observed in the NIR-II probe solution. This may be attributed to a decrease in the binding efficiency between the dye and protein at higher reaction concentrations, leading to aggregation of dye molecules that did not fully bind with albumin. This aggregation resulted in quenching and non-linear changes in fluorescence intensity (Figs. S9b-d in Supporting information).

The advantage of our covalent encapsulation strategy is that the structure of the prepared NIR-II fluorescent probes has precise molecular weight and spatial configuration, allowing for further investigation and optimization of its pharmacokinetics and potential toxicity, which is crucial for future clinical translation. To further understand this enhancement from a theoretical perspective, we performed docking simulations to analyze the binding interactions between different dyes and HSA (Fig. 1e and Fig. S10a in Supporting information). From the docking score and binding energy metrics (Figs. 1f and g, Figs. S10b and c in Supporting information), it is evident that C7–1080 can achieve more efficient binding with HSA, correlating with its highest brightness. Subsequently, we analyzed different HSA@Dyes probes using SDS-PAGE electrophoresis (Fig. 1h). The results showed that at the corresponding molecular weight position of albumin, C7–1080 exhibited a protein band with brightness significantly higher than that of the other dyes, with almost no free dye band present. This further confirms the efficient covalent binding between C7–1080 and albumin.

After confirming the strong binding ability of C7–1080 with HSA, we conducted a detailed analysis of the binding domains between HSA and C7–1080. Albumin is a versatile protein known for its ability to bind a wide range of small molecules, playing an important role in maintaining osmotic pressure and transporting various endogenous/exogenous substances. Albumin has multiple binding sites that can interact with diverse small molecules, including fatty acids, drugs, and dyes [36–39]. HSA can be divided into three distinct domains: domain I (DI), domain II (DII), and domain III (DIII). We incubated recombinant DI, DII, and DIII proteins with C7–1080 to investigate where the covalent binding occurs (Fig. 2a). The domain binding results showed that the fluorescence enhancement effect after incubation with DI and DII was very weak, while the enhancement effect after incubation with DIII was close to that of HSA (Fig. 2b). Theoretical simulations using gliding docking mode indicated that DIII had docking scores and binding energies closer to those of HSA, suggesting that the binding of C7–1080 is likely to occur in DIII (Figs. 2c-e). Subsequent SDS-PAGE analysis further confirmed these findings (Fig. 2f). DI@C7–1080 and DII@C7–1080 showed only free dye bands in the SDS-PAGE analysis. Conversely, DIII@C7–1080 resulted in a protein band with brightness similar to that of HSA@C7–1080, indicating that the covalent binding of C7–1080 with HSA primarily occurs in DIII rather than DI or DII.

High-resolution mass spectrometry (HRMS) can precisely detect and quantify whether the target small molecules covalently graft to protein, which can provide detailed structural information and determine complex mixtures from a stoichiometric perspective. We thus performed HRMS to analyze the binding efficiency of C7–1080 with the different domains (Figs. 2g-i and Fig. S12 in Supporting information). DI and DII exhibited negligible binding ratios of 2.08 % and 7.63 %, respectively, while DIII showed a significant binding ratio of 86.30 %. Therefore, we conclude that the covalent binding site of C7–1080 with HSA is located in DIII.

Traditionally, hydrophobic dyes are encapsulated with amphiphilic surfactants or polymers, such as DSPE-PEG, which significantly improve dye solubility in aqueous environments [32,33]. In this case, a micelle-like structure is formed, with the hydrophobic dye is sequestered in the core, while the hydrophilic chains extend outward. This encapsulation enhances the biocompatibility and circulation time of the dyes, providing a wide range of biomedical applications such as imaging and drug delivery. We therefore compared two different encapsulation strategies on C7–1080: our protein covalent encapsulation strategy and the classical encapsulation of the dye in amphiphilic surfactants or polymers to form nanoparticles (Fig. 3a). First, in terms of solution brightness, the HSA@C7–1080 probes exhibited significantly higher brightness than nanoparticles composed of surfactants and C7–1080 (Figs. 3b and c), under the same incubation condition (60 °C for 2 h). To evaluate the universality of the covalent encapsulation strategy, we conducted a comparative experiment using several NIR-II dyes mentioned earlier. Results indicated that the covalent encapsulation strategy demonstrated significantly superior NIR-II luminescent performance compared to non-covalent strategies in dyes with obvious covalent binding capabilities, such as Et-1080, FD-1080 and C7–1080. Besides, for dyes lacking strong covalent binding capabilities, albumin could also effectively encapsulate the dyes within the protein cavity through supramolecular interactions, providing luminescent performance comparable to those achieved with amphiphilic polymers like DSPE-PEG (Fig. S11 in Supporting information).

As we known, the biosafety and biocompatibility are also important indicators for evaluating whether an encapsulation strategy is suitable for biomedical applications. In cytotoxicity assays (Fig. 3d and Fig. S13 in Supporting information), among the three complexes with the highest brightness: HSA@C7–1080, DSPE-PEG@C7–1080, and CTAB@C7–1080, the CTAB@C7–1080 solution showed extremely high cytotoxicity, indicating its unsuitability for *in vivo* applications. In contrast, HSA@C7–1080 demonstrated superior biocompatibility. Besides, we also analyzed the microscopic morphologies of DSPE-PEG@C7–1080 and HSA@C7–1080 using dynamic light scattering (DLS) and transmission electron microscopy (TEM) (Figs. 3e-g). Results showed that both HSA@C7–1080 and DSPE-PEG@C7–1080 formed nanoparticles; however, the HSA@C7–1080 nanoparticle exhibited a lower polydispersity index (PDI) and smaller particle size compared to DSPE-PEG@C7–1080 nanoparticle. Therefore, the covalent encapsulation strategy by dye-protein binding was more controllable than the non-covalent encapsulation by polymer methods. Collectively, the covalent encapsulation approach offers superior luminescent properties and better biocompatibility, making it promising for *in vivo* applications.

To validate the effectiveness of our covalent encapsulation strategy *in vivo*, we compared the pure C7–1080 dye, DSPE-PEG@C7–1080 nanoparticle, and HSA@C7–1080 NIR-II fluorescent probe across different *in vivo* imaging models. First, to verify whether HSA@C7–1080 could effectively detect the lymphatic system *in vivo*, we injected three probes *via* the footpad and gently pressed the mouse footpad for 1 min to promote probe migration within the lymphatic system. Results showed that the HSA@C7–1080 was superior to C7–1080 and DSPE-PEG@C7–1080 in tracing lymph nodes and delineating lymphatic vessels (Fig. 4a). Notably, using the HSA@C7–1080, we successfully achieved precise lymph node dissection under NIR-II fluorescence guidance (Fig. 4b).

High-resolution vascular imaging is crucial for accurately assessing the success and integrity of postoperative vascular reconstruction [45,46]. It enables detailed visualization of blood vessels, allowing clinicians to detect any anomalies, such as blockages, leaks, or improper healing, which are critical for ensuring the long-term efficacy of the surgical procedure and for planning follow-up treatments. Our previous protein-escaping dye had the limitation of a very short imaging window for this purpose [45]. We thus compared the vascular imaging capabilities of the three different probes in healthy mice following tail vein injection. It

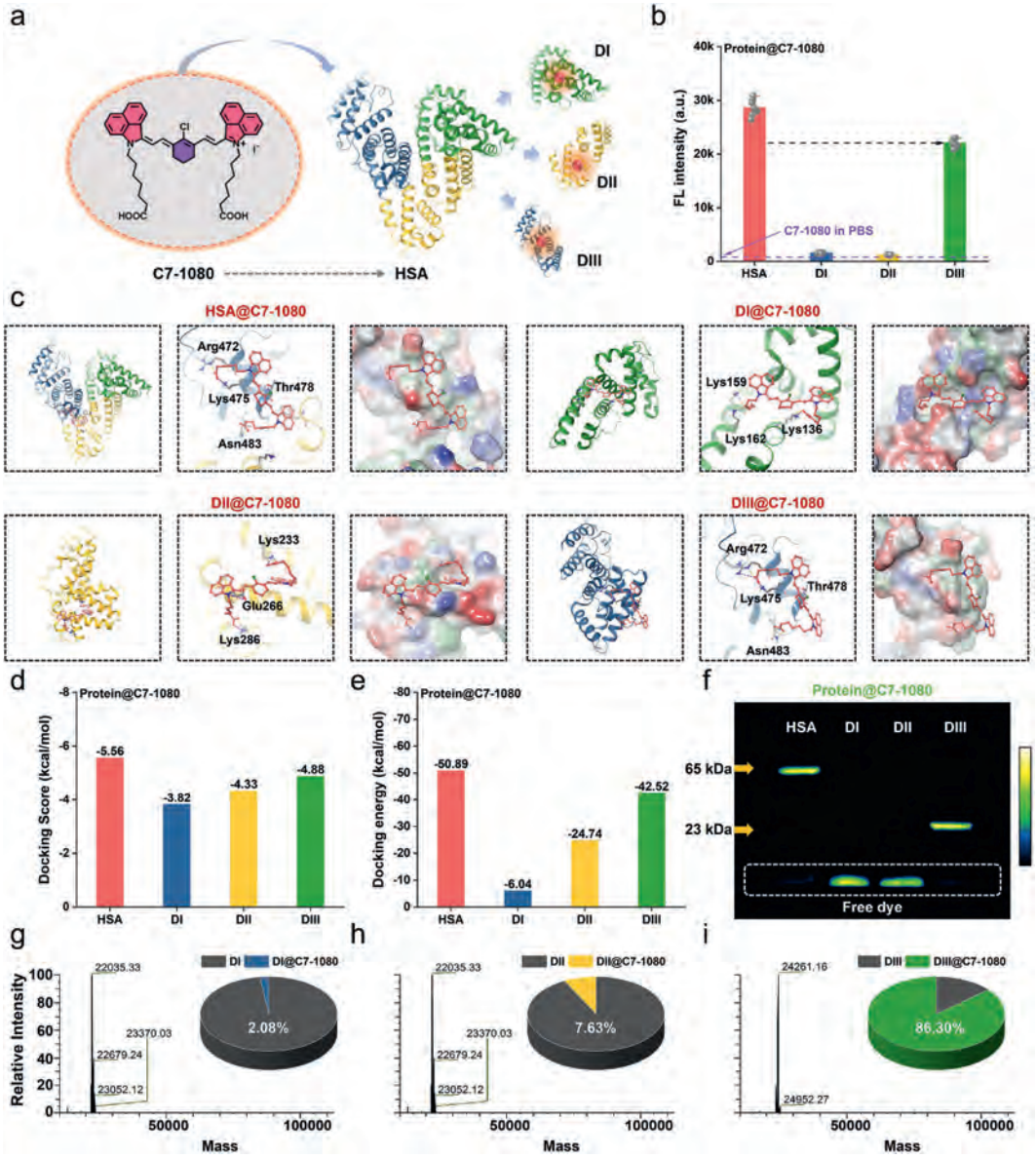


Fig. 2. Specific binding behavior between HSA and C7–1080. (a) Schematic of covalent binding between HSA and C7–1080. (b) NIR-II brightness after binding C7–1080 with HSA, DI, DII, and DIII. (c) Theoretical simulation of C7–1080 binding to HSA, DI, DII, DIII by gliding docking mode. (d, e) Comparison of docking score and binding energy between C7–1080 and HSA, DI, DII, DIII. (f) Gel electrophoresis analysis of the binding ability between C7–1080 and HSA, DI, DII, DIII. (g-i) High resolution mass spectrometry of the DI@C7–1080, DII@C7–1080 and DIII@C7–1080.

was evident that the vessels of mice injected with C7–1080 and DSPE-PEG@C7–1080 appeared significantly darker than those injected with HSA@C7–1080, making it difficult to visualize and distinguish the vessels. The vascular signal from HSA@C7–1080 was much higher than the background, allowing for clear differentiation. Moreover, HSA@C7–1080 also demonstrated excellent performance in brain and thigh vascular imaging. As the imaging window gradually red-shifted, the imaging quality improved, particularly in the wavelength ranges above 1400 nm and 1500 nm, where the background signal nearly disappeared (Fig. S14 in Supporting information). Consequently, we utilized HSA@C7–1080 to achieve high-resolution and high-contrast visualization of small vessels on the flap during the orthotopic flap transplantation. It could assist surgeons in avoiding damage to healthy vessels during the procedure (Fig. 4e and Fig. S15a in Supporting information) and help assess the vascular reconstruction effects after the flap transplantation in mice (Fig. 4f and Fig. S15b in Supporting information).

Besides, the neuro-fluorescence imaging aids surgeons in accurately locating nerve structures to prevent accidental damage to critical nerves, as well as better evaluating the extent and severity of nerve injury [47–49]. When assessing the neuroimaging performance of three probes (C7–1080, DSPE-PEG@C7–1080 and HSA@C7–1080) against the mouse sciatic nerve, the HSA@C7–1080 again exhibited superior imaging results (Figs. 4g and h, Fig. S16a in Supporting information). Meanwhile, we also attempted to evaluate the damage to the sciatic nerve using HSA@C7–1080 (Fig. 4j and Fig. S16b in Supporting information), in which we observed a significant reduction in the fluorescence signals near specific points on the injured nerve (Fig. 4i), indicating the potential site of nerve injury. Additionally, the pathological section results also effectively confirmed the presence of nerve damage (Fig. S16c in Supporting information).

In summary, this study developed a NIR-II cyanine dye molecule, C7–1080, that could efficiently bind to albumin. Us-

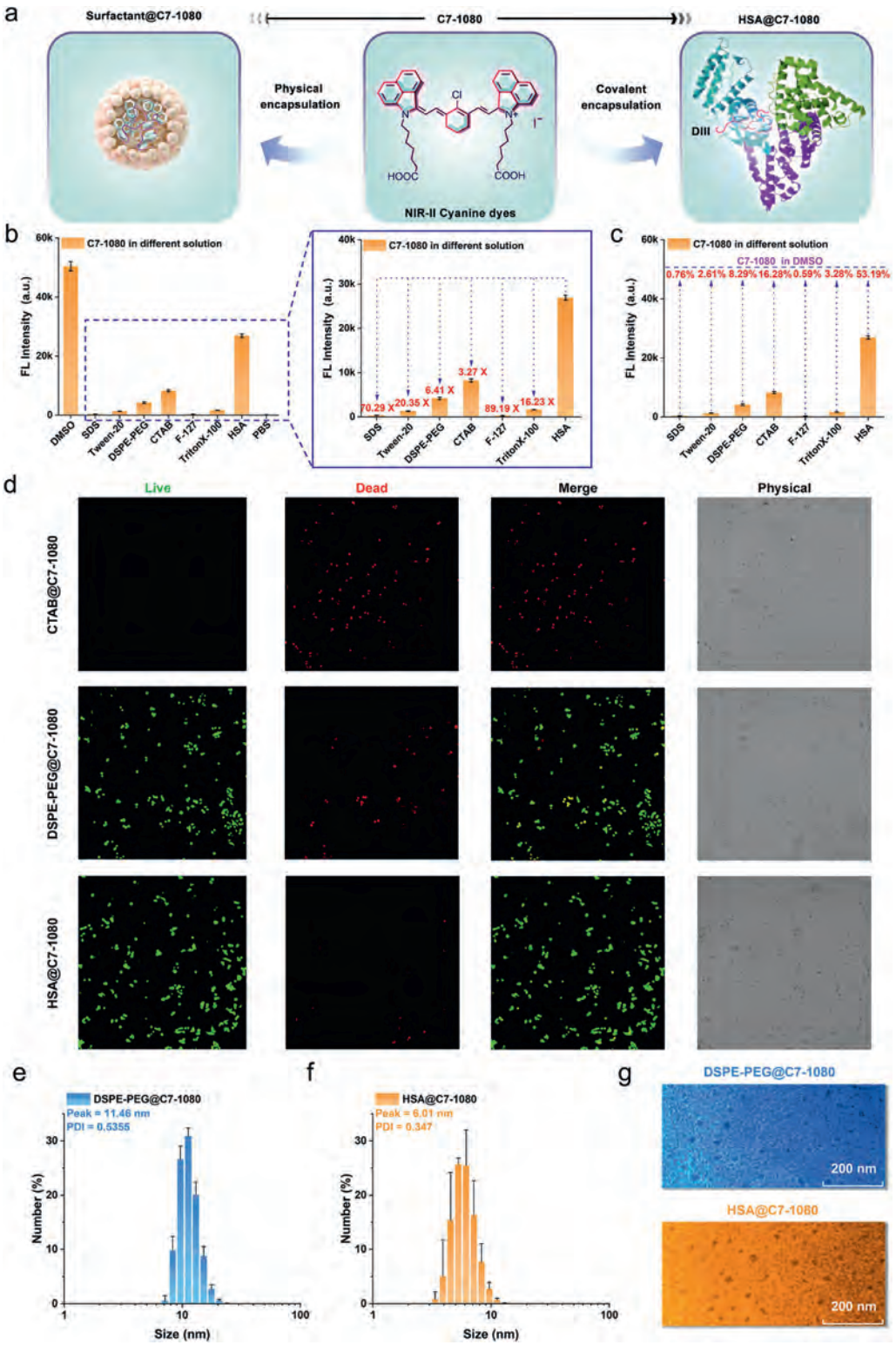


Fig. 3. Comparison of two different encapsulation strategies for C7–1080. (a) Schematic illustration of different encapsulation strategies for C7–1080: Non-covalent encapsulation (left) and covalent encapsulation (right). (b) NIR-II brightness comparison of HSA@C7–1080 and C7–1080 in different surfactant containing solution (the concentration ratio of surfactant to C7–1080 is 50:1). (c) Fluorescence retention comparison of C7–1080 in different surfactant solutions with that in DMSO. (d) Live-dead cell staining for CTAB@C7–1080, DSPE-PEG@C7–1080, and HSA@C7–1080 complexes. (e, f) Dynamic light scattering (DLS) analysis of DSPE-PEG@C7–1080 and HSA@C7–1080. (g) Transmission electron microscopy (TEM) images of DSPE-PEG@C7–1080 and HSA@C7–1080.

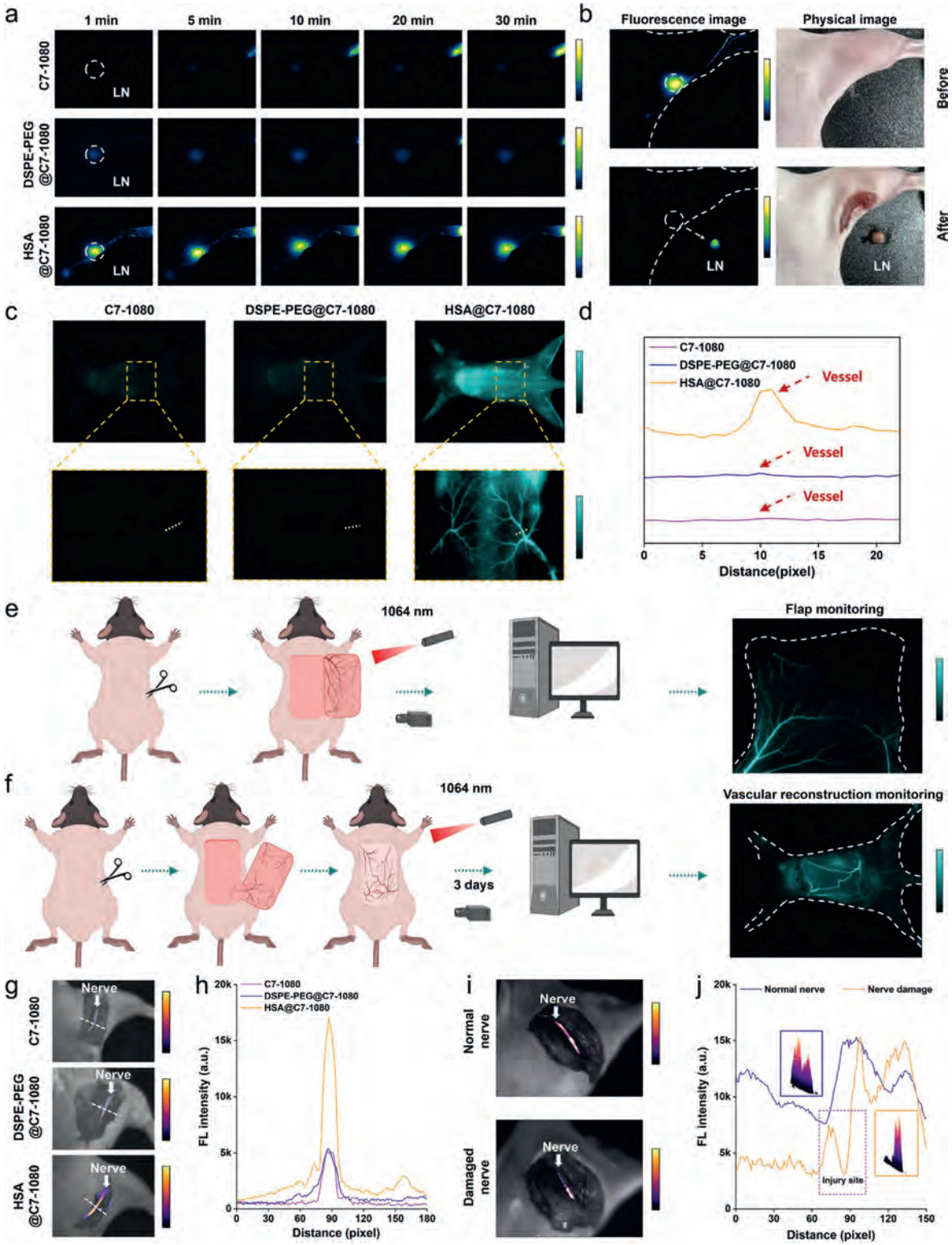


Fig. 4. *In vivo* imaging behavior of C7–1080, DSPE-PEG@C7–1080, and HSA@C7–1080. (a) NIR-II fluorescence imaging of lymph nodes at different time points after dye injection (Exposure time: 10 ms; Dosage: 25 μL (200 μmol/L)). (b) NIR-II fluorescence guided lymph node surgical excision using the HSA@C7–1080. (c) NIR-II imaging of dorsal blood vessels after intravenous injections of different dyes including C7–1080, DSPE-PEG@C7–1080, and HSA@C7–1080 (Exposure time: 80 ms; Dosage: 200 μL (600 μmol/L)). (d) Fluorescent cross-sectional intensity profile of vessels along the white dashed lines in Fig. 4c. (e) Schematic diagram of vascular imaging for monitoring flap transplantation and NIR-II fluorescence imaging of flap after intravenous injection of HSA@C7–1080 (Dosage: 200 μL (600 μmol/L)). (f) Schematic diagram of monitoring the vascular reconstruction of the mouse flap model with HSA@C7–1080 and NIR-II fluorescence imaging of reconstructed flap vessels after intravenous injection of HSA@C7–1080 (Dosage: 200 μL (600 μmol/L)). (g) NIR-II fluorescence imaging of the mouse sciatic nerve (Exposure time: 20 ms; Dosage: 3 μL (600 μmol/L)). (h) Fluorescent cross-sectional intensity profile of nerves along the white dashed lines in Fig. 4g. (i) Assessment of nerve damage with HSA@C7–1080. (j) Fluorescent intensity profile along the nerves in Fig. 4i. For all fluorescent imaging, Laser excitation: 1064 nm with 65 mW/cm^2; Filter: 1200 nm long-pass filters.

ing the brand-new synthetic C7–1080, we optimized the protein covalent encapsulation strategy and successfully constructed the HSA@C7–1080 NIR-II fluorescent probe. Compared to the existing NIR-II cyanine dyes, C7–1080 exhibited a greater propensity for covalent binding with albumin, resulting in the enhanced NIR-II fluorescence and photostability of HSA@C7–1080. Notably, in contrast to traditional delivery strategies that relied on the non-covalent assembly of amphiphilic polymers and organic small-molecule dyes, our approach enabled precise 1:1 controlled binding between dyes and proteins. The protein covalent encapsulation strategy effectively addressed the aggregation-induced quenching (ACQ) frequently observed in non-covalent assemblies, significantly improving the fluorescence efficiency of probes. Meanwhile, the HSA@C7–1080 also successfully achieved high resolution and contrast *in vivo* visualization of blood vessels, lymph, and nervous system. Collectively, the aforementioned strategy of optimizing small-molecule dye structures to modulate their binding behavior with proteins was expected to enrich the existing NIR-II fluorophore repertoire. With the recent advancements in fluorescence-guided surgery (FGS) in clinical settings [6–8], these high-performance fluorescent imaging agents would greatly improve the efficacy of FGS, providing deeper tissue penetration, higher spatial-temporal resolution, and more stable optical imaging outcomes. However, further preclinical evaluations and clinical trials would also be necessary for successful clinical translation.

Declaration of competing interest

The authors declare that they have no known competing financial interests or personal relationships that could have appeared to influence the work reported in this paper.

CRediT authorship contribution statement

Zijian Jiang: Writing – review & editing, Writing – original draft, Validation, Methodology, Investigation, Formal analysis, Data curation, Conceptualization. **Yijing Du:** Writing – review & editing, Resources, Methodology, Investigation, Data curation. **Zetao Dang:** Writing – review & editing, Resources, Investigation, Formal analysis. **Tongze Liu:** Methodology, Investigation. **Mengyuan Liu:** Methodology, Formal analysis. **Bin Sun:** Resources, Methodology. **Feiran Zhang:** Writing – review & editing, Validation, Supervision, Methodology, Conceptualization. **Jiajun Xu:** Writing – review & editing, Validation, Supervision, Project administration, Investigation, Data curation, Conceptualization. **Shoujun Zhu:** Writing – review & editing, Supervision, Funding acquisition, Conceptualization.

Acknowledgments

This work was supported by the National Key Research and Development Program of China (No. 2022YFC2408100), the National Science Foundation of Hebei Province (No. H2024201023), the Hebei Province Innovation Capability Enhancement Plan Project (No. 22567632H), the Research Project of Hebei Provincial Department of Education (No. BJ2025216), the Fund for Director of Key Laboratory of Medicinal Chemistry and Molecular Diagnosis of the Ministry of Education (No. MCMDZR-2024005), and the Fundamental Research Funds for the Central Universities of China.

Supplementary materials

Supplementary material associated with this article can be found, in the online version, at doi:10.1016/j.cclet.2025.111351.

References

[1] M. Wang, C. Wu, D. Sinefeld, et al., Biomed. Opt. Express 9 (2018) 3534–3543.
[2] N.G. Horton, K. Wang, D. Kobat, et al., Nat. Photon. 7 (2013) 205–209.
[3] G. Hong, A.L. Antaris, H. Dai, Nat. Biomed. Eng. 1 (2017) 0010.
[4] G. Hong, S. Diao, J. Chang, et al., Nat. Photon. 8 (2014) 723–730.
[5] S.L. Jacques, Phys. Med. Biol. 58 (2013) R37–R61.
[6] Y. Wu, Y. Suo, Z. Wang, et al., Front. Bioeng. Biotechnol. 10 (2022).
[7] Z. Hu, C. Fang, B. Li, et al., Nat. Biomed. Eng. 4 (2019) 259–271.
[8] Z. Zhang, Y. Du, X. Shi, et al., Nat. Rev. Clin. Oncol. 21 (2024) 449–467.
[9] J.A. Carr, T.A. Valdez, O.T. Bruns, et al., Proc. Natl. Acad. Sci. U. S. A. 113 (2016) 9989–9994.
[10] K. Welsher, Z. Liu, S.P. Sherlock, et al., Nat. Nanotech. 4 (2009) 773–780.
[11] K. Welsher, S.P. Sherlock, H. Dai, Proc. Natl. Acad. Sci. U. S. A. 108 (2011) 8943–8948.
[12] F. Wang, L. Qu, F. Ren, et al., Proc. Natl. Acad. Sci. U. S. A. 119 (2022) e2123111119.
[13] F. Wang, F. Ren, Z. Ma, et al., Nat. Nanotech. 17 (2022) 653–660.
[14] G. Hong, J.C. Lee, J.T. Robinson, et al., Nat. Med. 18 (2012) 1841–1846.
[15] F. Ren, F. Wang, A. Baghdasaryan, et al., Nat. Biomed. Eng. 8 (2023) 726–739.
[16] A.L. Antaris, H. Chen, K. Cheng, et al., Nat. Mater. 15 (2016) 235–242.
[17] B. Li, L. Lu, M. Zhao, et al., Angew. Chem. Int. Ed. 57 (2018) 7483–7487.
[18] Y. Zhu, F. Wu, B. Zheng, et al., Nano Lett. 24 (2024) 8287–8295.
[19] Y. Su, B. Yu, S. Wang, et al., Biomaterials 271 (2021) 120717.
[20] Y. Sun, C. Qu, H. Chen, et al., Chem. Sci. 7 (2016) 6203–6207.
[21] Y.Y. Duo, L. Zhao, Z.G. Wang, et al., J. Anal. Test. 7 (2023) 245–259.
[22] R.S. Gamage, D.H. Li, C.L. Schreiber, et al., ACS Omega 6 (2021) 30130–30139.
[23] S. Thavornpradit, S.M. Usama, G.K. Park, et al., Theranostics 9 (2019) 2856–2867.
[24] E.D. Cosco, A.L. Spearman, S. Ramakrishnan, et al., Nat. Chem. 12 (2020) 1123–1130.
[25] S. He, J. Song, J. Qu, et al., Chem. Soc. Rev. 47 (2018) 4258–4278.
[26] F. Wang, Y. Zhong, O. Bruns, et al., Nat. Photon. (2024) 535–547.
[27] B. Sun, K.S. Hettie, S. Zhu, Adv. Ther. 4 (2021) 2000278.
[28] W.S. Tummers, J.M. Warram, K.E. Tipirneni, et al., Cancer Res. 77 (2017) 2197–2206.
[29] F. Ding, C. Li, Y. Xu, et al., Adv. Healthc. Mater. 7 (2018) 1800973.
[30] H. Ma, C. Liu, Z. Hu, et al., Chem. Mater. 32 (2020) 2061–2069.
[31] R. Bhavane, Z. Starosolski, I. Stupin, et al., Sci. Rep. 8 (2018) 14455.
[32] H. Xu, L. Yuan, Q. Shi, et al., Nano Lett. 24 (2024) 1367–1375.
[33] X. Zhou, Y. Fan, S. Li, et al., Nano Lett. 24 (2024) 1792–1800.
[34] X. Zhu, C. Liu, Z. Hu, et al., Nano Res. 13 (2020) 2570–2575.
[35] Y. Shamay, J. Shah, M. Işık, et al., Nat. Mater. 17 (2018) 361–368.
[36] F. Kratz, B. Elsadek, J. Control. Release 161 (2012) 429–445.
[37] S. Rhaese, H. von Briesen, H. Rübsamen-Waigmann, et al., J. Control. Release 92 (2003) 199–208.
[38] B. Elsadek, F. Kratz, J. Control. Release 157 (2012) 4–28.
[39] M.J. Hawkins, P. Soon-Shiong, N. Desai, Adv. Drug Deliv. Rev. 60 (2008) 876–885.
[40] Q. Su, Y. Zhang, S. Zhu, Chem. Commun. 59 (2023) 13125–13138.
[41] S.M. Usama, K. Burgess, Acc. Chem. Res. 54 (2021) 2121–2131.
[42] Y. Xu, C. Yang, Y. Wu, et al., Nano Lett. 23 (2023) 5731–5737.
[43] S. Zhu, B.C. Yung, S. Chandra, et al., Theranostics 8 (2018) 4141–4151.
[44] J. Xu, N. Zhu, Y. Du, et al., Nat. Commun. 15 (2024) 2845.
[45] Y. Du, J. Xu, X. Zheng, et al., Adv. Mater. 36 (2024) 2311515.
[46] M.Y. Nahabedian, Clin. Plast. Surg. 38 (2011) 165–174.
[47] L.G. Wang, C.W. Barth, C.H. Kitts, et al., Sci. Transl. Med. 12 (2020) eaay0712.
[48] Q. Qu, H. Nie, S. Hou, et al., Eur. J. Nucl. Med. Mol. Imaging 49 (2022) 4752–4754.
[49] Z. Feng, Y. Yang, J. Zhang, et al., Nano Res. 12 (2019) 3059–3068.